

ARGO-YBJ OBSERVATION OF THE LARGE SCALE COSMIC RAY ANISOTROPY DURING THE SOLAR MINIMUM BETWEEN CYCLES 23 AND 24

B. BARTOLI^{1,2}, P. BERNARDINI^{3,4}, X.J. BI⁵, Z. CAO⁵, S. CATALANOTTI^{1,2}, S.Z. CHEN⁵, T.L. CHEN⁶, S.W. CUI^{7,*}, B.Z. DAI⁸, A. D'AMONE^{3,4}, DANZENGLUOBU⁶, I. DE MITRI^{3,4}, B. D'ETTORRE PIAZZOLI^{1,2}, T. DI GIROLAMO^{1,2}, G. DI SCIASCIO⁹, C.F. FENG¹⁰, ZHAOYANG FENG⁵, ZHENYONG FENG¹¹, W. GAO⁷, Q.B. GOU⁵, Y.Q. GUO⁵, H.H. HE⁵, HAIBING HU⁶, HONGBO HU⁵, M. IACOVACCI^{1,2}, R. IUPPA^{9,12}, H.Y. JIA¹¹, LABACIREN⁶, H.J. LI⁶, C. LIU⁵, J. LIU⁸, M.Y. LIU⁶, H. LU⁵, L.L. MA⁵, X.H. MA⁵, G. MANCARELLA^{3,4}, S.M. MARI^{13,14}, G. MARSELLA^{3,4}, S. MASTROIANNI², P. MONTINI⁹, C.C. NING⁶, L. PERRONE^{3,4}, P. PISTILLI^{13,14}, P. SALVINI¹⁵, R. SANTONICO^{9,12}, P.R. SHEN⁵, X.D. SHENG⁵, F. SHI⁵, A. SURDO⁴, Y.H. TAN⁵, P. VALLANIA^{16,17}, S. VERNETTO^{16,17}, C. VIGORITO^{17,18}, H. WANG⁵, C.Y. WU⁵, H.R. WU⁵, L. XUE¹⁰, Q.Y. YANG⁸, X.C. YANG⁸, Z.G. YAO⁵, A.F. YUAN⁶, M. ZHA⁵, H.M. ZHANG⁵, L. ZHANG⁸, X.Y. ZHANG¹⁰, Y. ZHANG⁵, J. ZHAO⁵, ZHAXICIREN⁶, ZHAXISANGZHU⁶, X.X. ZHOU¹¹, F.R. ZHU¹¹, AND Q.Q. ZHU⁵
(THE ARGO-YBJ COLLABORATION)

¹Dipartimento di Fisica dell'Università di Napoli "Federico II", Complesso Universitario di Monte Sant'Angelo, via Cinthia, 80126 Napoli, Italy.

²Istituto Nazionale di Fisica Nucleare, Sezione di Napoli, Complesso Universitario di Monte Sant'Angelo, via Cinthia, 80126 Napoli, Italy.

³Dipartimento Matematica e Fisica "Ennio De Giorgi", Università del Salento, via per Arnesano, 73100 Lecce, Italy.

⁴Istituto Nazionale di Fisica Nucleare, Sezione di Lecce, via per Arnesano, 73100 Lecce, Italy.

⁵Key Laboratory of Particle Astrophysics, Institute of High Energy Physics, Chinese Academy of Sciences, P.O. Box 918, 100049 Beijing, P.R. China.

⁶Tibet University, 850000 Lhasa, Xizang, P.R. China.

⁷Hebei Normal University, 050024, Shijiazhuang Hebei, P.R. China.

⁸Yunnan University, 2 North Cuihu Rd., 650091 Kunming, Yunnan, P.R. China.

⁹Istituto Nazionale di Fisica Nucleare, Sezione di Roma Tor Vergata, via della Ricerca Scientifica 1, 00133 Roma, Italy.

¹⁰Shandong University, 250100 Jinan, Shandong, P.R. China.

¹¹Southwest Jiaotong University, 610031 Chengdu, Sichuan, P.R. China.

¹²Dipartimento di Fisica dell'Università di Roma "Tor Vergata", via della Ricerca Scientifica 1, 00133 Roma, Italy.

¹³Dipartimento di Fisica dell'Università "Roma Tre", via della Vasca Navale 84, 00146 Roma, Italy.

¹⁴Istituto Nazionale di Fisica Nucleare, Sezione di Roma Tre, via della Vasca Navale 84, 00146 Roma, Italy.

¹⁵Istituto Nazionale di Fisica Nucleare, Sezione di Pavia, via Bassi 6, 27100 Pavia, Italy.

¹⁶Osservatorio Astrofisico di Torino dell'Istituto Nazionale di Astrofisica, via P. Giuria 1, 10125 Torino, Italy.

¹⁷Istituto Nazionale di Fisica Nucleare, Sezione di Torino, via P. Giuria 1, 10125 Torino, Italy.

¹⁸Dipartimento di Fisica dell'Università di Torino, via P. Giuria 1, 10125 Torino, Italy.

ApJ, in press

ABSTRACT

This paper reports on the measurement of the large scale anisotropy in the distribution of cosmic ray arrival directions using the data collected by the air shower detector ARGO-YBJ from 2008 January to 2009 December, during the minimum of solar activity between cycles 23 and 24. In this period more than 2×10^{11} showers were recorded, with energies between ~ 1 and 30 TeV. The observed two-dimensional distribution of cosmic rays is characterized by two wide regions of excess and deficit, respectively, both of relative intensity $\sim 10^{-3}$ with respect to a uniform flux, superimposed to smaller size structures. The harmonic analysis shows that the large scale cosmic ray relative intensity as a function of right ascension can be described by the first and second terms of a Fourier series. The high event statistics allows the study of the energy dependence of the anisotropy, showing that the amplitude increases with energy, with a maximum intensity at ~ 10 TeV, then it decreases, while the phase slowly shifts towards lower values of right ascension with increasing energy. The ARGO-YBJ data provide accurate observations over more than a decade of energy around this feature of the anisotropy spectrum.

Keywords: Cosmic-Ray, Large Scale Anisotropy, EAS Array

1. INTRODUCTION

The first observations showing that the arrival directions of Very High Energy Cosmic Rays (VHE CRs, $E > 100$ GeV) are not isotropically distributed were made in 1932, soon after the discovery of CRs, but only in the '50s, underground and surface detectors could provide the clear evidence of a sidereal anisotropy, with intensity $10^{-4} - 10^{-3}$ with respect to the isotropic background. The detectors measured the anisotropy as a variation of the cosmic ray flux over the sidereal day, and on the basis of a harmonic analysis, the data from different experiments were compared in terms of the amplitudes and

phases of the lowest order harmonics.

In 1998, by combining the data from different experiments operating in the primary energy range $\sim 0.1-10$ TeV and located in the northern and southern hemisphere, two structures were recognized: an excess close to the direction of the helio-tail (which has since been referred to as the "tail-in" excess) and a broad deficit towards the direction of the Galactic North Pole, which authors thought originated from a poloidal, cone-shaped component of the galactic magnetic field (since then, named the "loss-cone") (Nagashima et al. 1998).

In the last decade, ground-based and underground/under-ice experiments with great statistics and good angular resolution, provided two-dimensional representations of the CR arrival directions, allowing detailed morphological studies of

* Corresponding author: cuisw@ihep.ac.cn

the anisotropy structures. The new data concern both the northern hemisphere (Super Kamiokande, Tibet AS γ , Milagro, and ARGO-YBJ experiments) and the southern one (IceCube and IceTop experiments) (Amenomori et al. 2006; Guillian et al. 2007; Abdo et al. 2009; Zhang, J.L. et al. 2009; Abbasi et al. 2010, 2011, 2012; Aartsen et al. 2013). Although no systematic attempt has been made to merge all data to get a full-sky map of CRs, observations clearly depict a common large scale structure in the arrival direction distribution of CRs of energy less than 100 TeV. Dipole and quadrupole components mostly contribute to the “tail-in” (Right Ascension $\sim 50^\circ$ - 130°) and the “loss-cone” (R.A. $\sim 160^\circ$ - 240°). Narrower and less intense regions were also detected by the most sensitive experiments (Abdo et al. 2008; Abbasi et al. 2011; Bartoli et al. 2013; Abeyskara et al. 2014).

Of particular importance have been the results at higher energies by EAS-TOP (Aglietta et al. 2009), IceCube (Abbasi et al. 2012) and IceTop (Aartsen et al. 2013), that revealed a completely different scenario: a strong deficit at right ascension around 80° (relative intensity 2×10^{-3} and size about 35°) at energies ~ 400 TeV and ~ 2 PeV respectively, consistent with an abrupt phase variation of the first harmonics by ~ 10 hours of sidereal time at energy above ~ 400 TeV.

Concerning the energy dependence of the observed anisotropy, the intensity shows a tendency to increase from 0.1 to 10 TeV, whereas the phase slowly shifts of a few hours over the same energy interval. Between 10 and 100 TeV, results from (Amenomori et al. 2006) showed a progressively smaller amplitude. The Cascade collaboration did not detect any signal above 700 TeV (Antoni et al. 2004), whereas EAS-TOP, IceCube and IceTop detected modulations of increasing intensity above 400 TeV, accompanied by the above cited phase flip at ~ 400 TeV (Aglietta et al. 2009; Abbasi et al. 2012; Aartsen et al. 2013).

The temporal behaviour of the anisotropy is more controversial. While Milagro reported a steady increase of the intensity at a median energy of about 6 TeV during the years 2000-2007 (corresponding to a decrease of the solar activity) (Abdo et al. 2009), the Tibet AS γ experiment did not observe any significant difference of the anisotropy intensity at ~ 5 TeV in nine years of data from 1999 to 2008 (Amenomori et al. 2010, 2012). On the other hand a weak correlation between the anisotropy amplitude at energy ~ 0.6 TeV and the solar activity has been found in a 22 years muon data set (Munakata et al. 2010).

A number of explanations for the CR anisotropy have been proposed. Ingredients for a model are CR production, acceleration and propagation, which are considered together or independent of each other. The effect may simply relate to the uneven distribution of CR sources in the Galaxy or reflect propagation features that are not yet understood. The Galactic magnetic field and the local magnetic field, mostly in the heliosphere, likely play a major role in this area. If the heliosphere is one of the causes of the observed CR anisotropy, one could expect a time variation of the effect, related to the solar cycle.

Additionally, Compton and Getting predicted a dipolar anisotropy (never observed so far in sidereal time) due to the motion of the observer relative to the CR plasma. Assuming that CR do not co-rotate with the Galaxy (Compton & Getting 1935), there would be an excess of CR intensity from the direction of motion of the solar system, while a deficit would

appear in the opposite direction. Because of its purely kinematic origin, the Compton-Getting effect (CGE) is independent on the CR primary energy.

Recent works of Zhang et al. (2014) and Schwadron et al. (2014) discussed the local origin model of the anisotropies, while Qu et al. (2012) proposed a global galactic “CR Stream” model to understand the observation of the major anisotropic components in the solar vicinity. Some work focuses on the smaller scale anisotropies as the ones observed by Milagro (Abdo et al. 2008) and ARGO-YBJ (Bartoli et al. 2013), and attempts to explain that the excess could be related to the Geminga pulsar as a local cosmic-ray source (Salvati & Sacco 2010) or could be due to the magnetic mirror effect on CRs from a local source (Drury & Aharonian 2008). Many related studies are ongoing. However a generally accepted theory able to explain all the observations doesn’t exist yet, and more data are necessary to provide a solid ground for a firm theory.

This paper reports on the observations of the large scale anisotropy made by the air shower detector ARGO-YBJ from January 2008 to December 2009, during the minimum of solar activity between cycles 23 and 24. ARGO-YBJ was instrumented with a full-coverage “carpet” of particle detectors, a solution which significantly lowers the primary energy threshold and provides a high trigger rate. These features allowed the accurate investigation of the CR anisotropy over the energy range ~ 1 - 30 TeV. The choice to limit this work to the solar minimum period was to reduce any possible influence of the solar activity on the arrival distribution of cosmic rays. The study of the behaviour of the anisotropy during the years of increasing solar activity of cycle 24 is deferred to a future publication.

In this article, the experiment layout and the detector performance are reported in Section 2. Section 3 contains a description of the analysis technique. Section 4 reports the results in terms of two-dimensional maps and harmonic analysis in sidereal time. The energy dependence of the anisotropy is described and systematic uncertainties are discussed. A summary concludes the paper in the last section.

2. THE ARGO-YBJ EXPERIMENT

The ARGO-YBJ experiment is a full coverage air shower detector located at the Yangbajing Cosmic Ray Laboratory (Tibet, P.R. China, longitude 90.5° East, latitude 30.1° North) at an altitude of 4300 m above the sea level, devoted to gamma ray astronomy above ~ 300 GeV and cosmic ray studies above ~ 1 TeV.

The detector consists of a $\sim 74 \times 78$ m² carpet made of a single layer of Resistive Plate Chambers (RPCs) with $\sim 92\%$ of active area, surrounded by a partially instrumented ($\sim 20\%$) area up to $\sim 100 \times 110$ m². The apparatus has a modular structure, the basic data acquisition element being a cluster (5.7×7.6 m²), made of 12 RPCs (2.85×1.23 m²). Each RPC is read by 80 strips of 6.75×61.8 cm² (the spatial pixels), logically organized in 10 independent pads of 55.6×61.8 cm² which are individually acquired and represent the time pixels of the detector (Aiellia et al. 2006). To extend the dynamical range up to PeV energies, each RPC is equipped with two large size pads (139×123 cm²) to collect the total charge developed by the particles hitting the detector. The full experiment is made of 153 clusters (18360 pads), for a total active surface of ~ 6600 m².

ARGO-YBJ operates in two independent acquisition

modes: the *shower mode* and the *scaler mode*. In shower mode, all showers with a number of hit pads $N_{hits} \geq 20$ in the central carpet in a time window of 420 ns generate the trigger. The events collected in shower mode contain both the digital and the analog information on the shower particles. In this analysis we refer to the digital data recorded in shower mode.

The primary arrival direction is determined by fitting the arrival times of the shower front particles. The angular resolution for cosmic ray induced showers has been checked using the Moon shadow (i.e. the shadow cast by the Moon on the cosmic ray flux), observed by ARGO-YBJ with a statistical significance of ~ 9 standard deviations per month. The shape of the shadow provided a measurement of the detector PSF, that has been found in agreement with expectations. The angular resolution depends on N_{hits} (hereafter referred to as *pad multiplicity*) and varies from 0.3° for $N_{hits} > 1000$ to 1.8° for $N_{hits}=20-39$ (Bartoli et al. 2011).

The pad multiplicity is used as an estimator of the primary energy. The relation between the primary energy and the pad multiplicity is given by Monte Carlo simulations. The reliability of the energy scale has been tested with the Moon shadow. Due to the geomagnetic field, cosmic rays are deflected according to their energy and the Moon shadow is shifted with respect to the Moon position by an amount depending on the primary energy. The westward shift of the shadow has been measured for different N_{hits} intervals and compared to simulations. We found that the total absolute energy scale error is less than 13% in the proton energy range $\sim 1-30$ TeV, including the uncertainties on the cosmic ray elemental composition and the hadronic interaction model (Bartoli et al. 2011).

3. DATA SELECTION AND ANALYSIS TECHNIQUE

The full ARGO-YBJ detector was in stable data taking from 2007 November to 2013 February, with a trigger rate of ~ 3.5 kHz and an average duty cycle of $\sim 86\%$. For this analysis, the 2×10^{11} events recorded in 2008-2009 were selected according to the following requirements:

- (1) more than 40 pads fired in the central carpet: $N_{hits} \geq 40$;
- (2) shower zenith angle $\theta < 45^\circ$

About 3.6×10^{10} events survived the selection, with arrival directions in the declination band $-10^\circ < \delta < +70^\circ$.

The isotropic CR background was estimated via the equi-zenith (EZ) angle method, where the expected distribution was fitted to the experimental data by minimising the residuals with an iteration technique (Amenomori et al. 2005a). This approach undoubtedly presents the advantage that it can account for effects that are caused by instrumental and environmental variations, such as changes in pressure or temperature. The method assumes that the events are uniformly distributed in azimuth for a given zenith angle bin, or at least that gradients are stable over a long time, as is the case for ARGO-YBJ (Bartoli et al. 2014a).

Two sky maps are built with cells of $1^\circ \times 1^\circ$ in right ascension α and declination δ : the event map $N(\alpha_i, \delta_j)$ containing the detected events, and the background map $N_b(\alpha_i, \delta_j)$ containing the background events as estimated by the EZ method. The maps are smoothed to increase the statistical significance, i.e. for each map bin, the events inside a circle of radius 5° around that bin are summed.

Let $I_{i,j}$ denote the relative intensity in the sky cell (α_i, δ_j) , defined as the ratio of the number of detected events and the estimated background events:

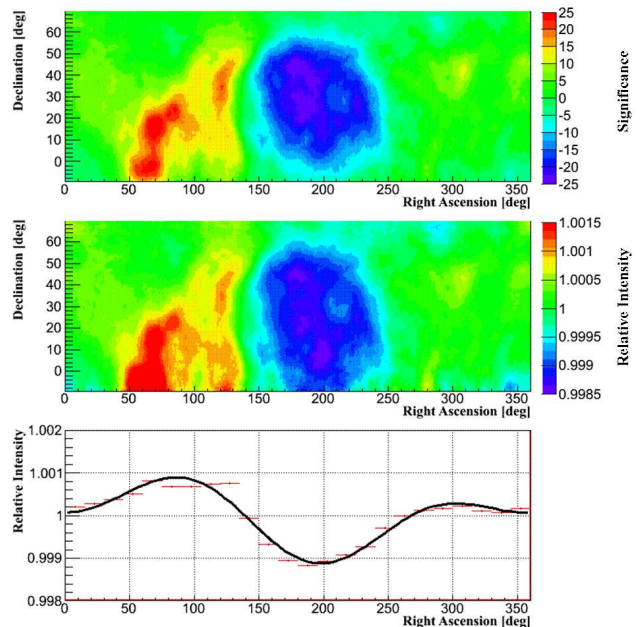


Figure 1. Upper panel: significance map of the cosmic ray relative intensity in the equatorial coordinate system, for events with $N_{hits} \geq 40$. Medium panel: relative intensity map. Lower panel: relative intensity as a function of the right ascension, integrated over the declination. The line represents the best fit curve obtained with the harmonic analysis. The abscissa bars present the wide of bins and the ordinate small error bars represent statistical errors.

$$I_{i,j} = \frac{N(\alpha_i, \delta_j)}{N_b(\alpha_i, \delta_j)} \quad (1)$$

The statistical significance s of the excess (or deficit) of cosmic rays with respect to the expected background is given by

$$s = \frac{I_{i,j} - 1}{\sigma_{I_{i,j}}} \quad (2)$$

where $\sigma_{I_{i,j}}$ is calculated from $N(\alpha_i, \delta_j)$ and $N_b(\alpha_i, \delta_j)$ taking into account the number of bins used to evaluate the average background with the EZ method.

4. SIDEREAL ANISOTROPY

The significance map of the excesses obtained by ARGO-YBJ using the events with $N_{hits} \geq 40$ is given in the first panel of Fig.1, while the corresponding map showing the relative intensity of cosmic rays is reported in the second panel of the same figure. According to simulations (see next subsection), the median energy of the selected events is 1.3 TeV.

Two distinct large structures are visible: a complex excess region at R.A. = $50^\circ-140^\circ$ (the so called “tail-in” excess) and a broad deficit at R.A. = $150^\circ-250^\circ$ (the “loss-cone”). A small diffuse excess around R.A. = 310° and $\delta = 40^\circ$ is also present, with a significance of about 13 standard deviations, corresponding to the Cygnus region, mostly due to gamma ray emission. The Cygnus region hosts a number of gamma-ray sources, plus an extended emission region detected by Fermi-LAT (Nolan et al. 2012) and ARGO-YBJ (Bartoli et al. 2014b), known as the “Cygnus Cocoon”. Since ARGO-YBJ cannot distinguish between cosmic ray and gamma ray showers, the map of Fig.1 also contains some excess due to gamma ray sources, like the Crab Nebula (R.A. = 83.6° , $\delta =$

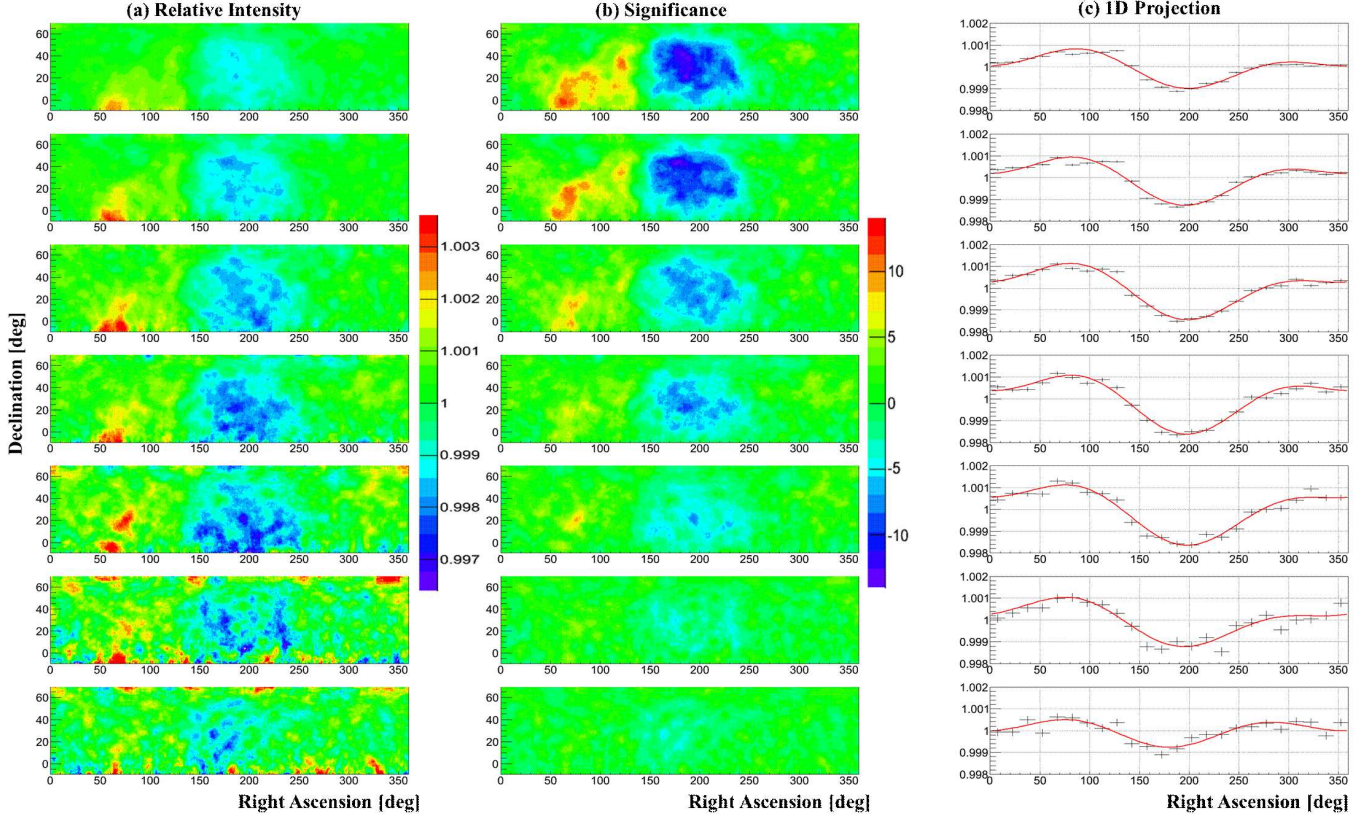


Figure 2. (a) Cosmic ray relative intensity maps for different N_{hits} intervals; from top to bottom, $N_{hits}=40-59, 60-99, 100-159, 160-299, 300-699, 700-999,$ and $N_{hits} \geq 1000$; (b) significance maps for the same N_{hits} intervals; (c) projection of the two-dimensional intensity maps onto the right ascension axis; the curves are the best fit functions obtained with the harmonic analysis. The error bars are statistical.

22.0°). The excesses due to gamma ray sources have a relative small statistical significance compared to the one reported by ARGO-YBJ in gamma ray studies (Bartoli et al. 2014c, 2015), because here the analysis parameters are not optimized for gamma ray measurements and the smoothing angle is much larger than the angular resolution for gamma rays. Since the excesses due to gamma rays are highly localized, they do not alter the large scale structure of the map.

The lower panel of Fig.1 shows the intensity as a function of the right ascension, obtained by projecting the two-dimensional map on the right ascension axis, in bins of 15°, and averaging over the declination values. Following the standard harmonic analysis procedure, we fit the projected intensity with the first two terms of the Fourier series:

$$I = 1 + A_1 \cos[2\pi(x - \phi_1)/360] + A_2 \cos[2\pi(x - \phi_2)/180], \quad (3)$$

where x is the right ascension.

The obtained bestfit amplitudes and phases of the two harmonics are: $A_1 = (6.8 \pm 0.06) \times 10^{-4}$, $A_2 = (4.9 \pm 0.06) \times 10^{-4}$, $\phi_1 = (39.1 \pm 0.46)^\circ$ and $\phi_2 = (100.9 \pm 0.32)^\circ$, with a $\chi^2/\text{d.o.f.} = 1273/20$.

The given errors are purely statistical. The poor $\chi^2/\text{d.o.f.}$ value is due to the simple fitting function, that is not able to describe the complex morphology of the map, in particular the right ascension region from 50° to 140°. Indeed, the fit does not improve substantially even by adding a third harmonic. More detailed analysis on these structures and their energy dependence have been discussed in (Bartoli et al. 2013). De-

spite the large χ^2 value due to the small structures superimposed to the smoother modulation, the figure shows that the general shape of the anisotropy can be described enough satisfactorily with two harmonics.

Our data, as previous measurements by other detectors, rule out the hypothesis that the sidereal Compton-Getting effect is the dominant anisotropy component. The Compton-Getting effect has a purely kinetic nature, and directly follows from the relative motion of the observer and the medium. If the velocity field is uniform, the intensity of the anisotropy depends on $\mathbf{v}(t) \cdot \mathbf{n}$, where $\mathbf{v}(t)$ is the velocity of the medium with respect to the observer and \mathbf{n} the observing direction. Assuming that cosmic rays do not co-rotate with the Galaxy (Amenomori et al. 2006), taking into account the Sun's orbital speed ($\sim 200 \text{ km s}^{-1}$), the CG effect predicts a dipole anisotropy of amplitude $A_{CG} = 3.5 \times 10^{-3}$, much larger than what we observe, with the maximum in the direction of the motion of the solar system around the Galactic Center, (i.e. R.A. = 315° and $\delta = 49^\circ$) and the minimum in the opposite direction, not consistent with the position of the excess and deficit regions observed in our analysis.

4.1. Anisotropy vs Energy

Recent and past observations of cosmic rays have shown that the anisotropy is energy dependent. Thanks to its high statistics, ARGO-YBJ can study separately the anisotropy in different energy ranges. We divided the data in seven subsets, according to the number of fired pad: $N_{hits}=40-59, 60-99, 100-160, 160-300, 300-700, 700-1000,$ and $N_{hits} \geq 1000$.

The median energy corresponding to the above intervals have been estimated by means of a Monte Carlo simulation. The showers were generated by the CORSIKA code v.6.502 (Heck et al. 1998) assuming a power law spectrum with a differential index $\alpha=-2.63$ (Bartoli et al. 2014d) and a primary energy ranging from 10 GeV to 1 PeV. The hadronic interactions at high energies are treated with the QGSJET-II model, while the low energy interactions with GHEISHA. A total of 2×10^8 events were sampled in the zenith angle band from 0° to 70° . A GEANT4 based detector simulation code was used to determine the detector response (Guo et al. 2009). The events were then selected according to the cuts used in the analysis of real data, and divided into seven samples according to the number of hits recorded by the detector. According to the simulations, the primary median energy corresponding to the different N_{hits} intervals are: 0.98, 1.65, 2.65, 4.21, 7.80, 13.6 and 29.1 TeV, respectively.

The left panel of Fig.2(a) shows the relative intensity maps for the seven N_{hits} intervals. Structures with complex morphologies are visible in all the maps, changing shape with energy. It has to be noted however that the structures at declinations $\delta < 0^\circ$ and $\delta > 60^\circ$ observed in the maps with $N_{hits} \geq 700$ are statistical fluctuations due to the limited statistics, as can be deduced by Fig.2(b), that shows the statistical significance of the same maps.

As for the total sky map, the harmonic analysis has been performed for the seven N_{hits} intervals, by using the projection of the two-dimensional maps onto the right ascension axis. The best-fit curves are shown in the right panel of Fig.2(c), while the obtained values of amplitudes and phases are summarized in Table 1.

According to this analysis, the first harmonic amplitude steadily increases for energy from ~ 1 TeV to ~ 10 TeV, after which it decreases. The amplitude almost doubles in less than one energy decade, then decreases to a smaller value for energies of ~ 20 -30 TeV. This trend is shown in the upper panel of Fig.3, that reports the found amplitudes as a function of the median primary energy, together with the results of other experiments covering the energy range ~ 100 GeV - 500 TeV (see Di Sciascio and Iuppa (2013) and references therein). All data agree on the existence of a maximum in the intensity around ~ 10 TeV.

The lower panel of Fig.3 shows the phase of the first harmonics as a function of energy. The phase values found by ARGO-YBJ are consistent with the general trend of a slow phase decrease with energy up to about 400 TeV, when an abrupt change of phase occurs.

From Table 1, one can see that the amplitude of the second harmonics is in general smaller than the first one. It shows a similar up-and-down trend with energy, but the percent variation is smaller: the amplitude increases by a factor ~ 1.5 in the energy interval 1-4 TeV, then decreases at higher energies.

The trends of the amplitude and phase found in the harmonic analysis reflect the energy dependence of the intensity maps of Fig.2. The absolute values of the minimum and maximum intensity increase with energy up to ~ 10 TeV, and decrease afterwards. At the same time, the regions of maximum and minimum intensity slightly shift towards lower right ascension values at the highest energies.

It is interesting to compare our data with the Tibet AS- γ array results given in Amenomori et al. (2012), that reports the amplitude of the “loss-cone” deficit during 8 years, from 2000 to 2007, for three values of the primary median energy (4.4,

6.2 and 11 TeV), compared with a Milagro measurement at 6 TeV performed in about the same time interval. According to Tibet AS- γ data, the deficit amplitude (defined as the difference between unity and the relative intensity at the minimum of the best-fit curve of the harmonic analysis) is stable during the period under study, with a value in the range ~ 0.0010 - 0.0013 , while the Milagro data show a linear increase of the amplitude with time, going from ~ 0.0014 in 2001 to ~ 0.0034 at the end of 2006. Our data, that closely follow in time the AS- γ and Milagro measurements, show a deficit amplitude in the range 0.0012-0.0016 for energies ~ 4 -14 TeV (see Fig.2(c)), in agreement with the Tibet results, not confirming the large increase observed by Milagro.

4.2. Systematic Uncertainties

Systematic errors in the sidereal analysis can be due to seasonal and diurnal effects, like atmospheric temperature and pressure variations that modify the cosmic ray rate and the detector efficiency, and that do not cancel out completely even using full-year data. Considering the small amplitude of the anisotropy, systematics must be carefully evaluated and taken under control.

A standard test to verify the absence of solar effects in sidereal measurements is the harmonic analysis in anti-sidereal time. The anti-sidereal time is an artificial time which has 364.25 cycles per year, one day less than the number of days in a year of solar time, and two days less than the number of sidereal days. In principle, the harmonic analysis in anti-sidereal time should find no anisotropy at all, since no physical phenomena exist with such a periodicity. However, if some effect in solar time affects the sidereal distribution, it will also affect the anti-sidereal one. The anti-sidereal analysis is a valid method to estimate such systematics, and if needed, to correct them (Guillian et al. 2007).

The results of the anti-sidereal analysis are reported in the last column of Table 1. The found amplitudes give a good estimation of the systematic uncertainty of the corresponding sidereal amplitudes for each N_{hits} interval. Since they are about 13% or less than the sidereal ones, a correction of the solar effects is not necessary for this analysis. As an example, the upper panel of Fig.4 reports the anti-sidereal distribution for $N_{hits} = 60$ -99. The lower panel shows that the effect of the correction on the sidereal analysis, performed according to the method described in Guillian et al. (2007), is negligible.

Further checks of the reliability of our data have been done exploiting the East-West method and the Compton Getting effect.

4.2.1. The East-West method

Before the late '90s, when experiments were not able to collect enough statistics to study the distribution of the CR arrival direction both in the right ascension and declination, measurements were performed exploiting the “East-West” method (Aglietta et al. 2009; Bonino et al. 2011). This method is based on a differential approach: for each declination belt, the difference of the event rate measured at $+h$ and $-h$ hour angle is considered. If this quantity is studied as a function of the local sidereal time, the “derivative” of the sidereal anisotropy projection is obtained, and a simple integration gives the sidereal anisotropy. This analysis is based on the difference between the event rates recorded simultaneously from different directions, hence is free from systematics due to spurious rate variations. In the analysis presented here, h was calculated by

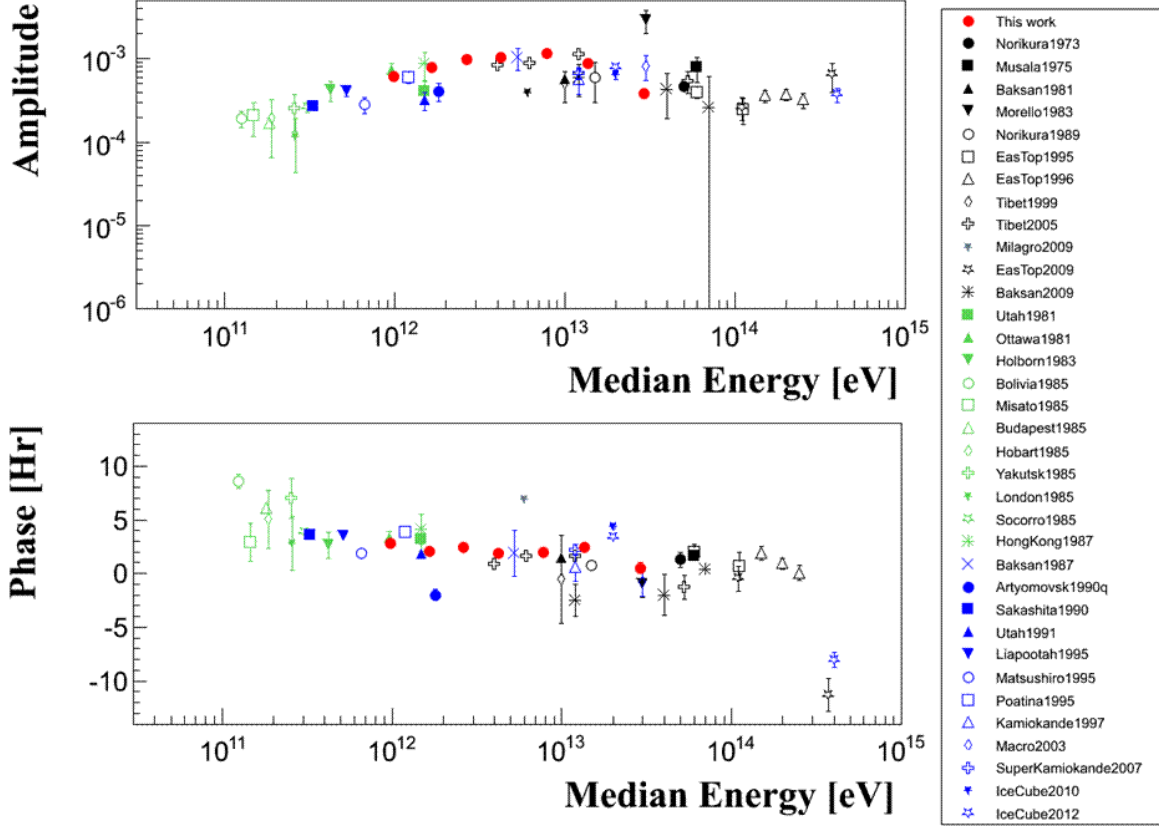


Figure 3. Amplitude (upper panel) and phase (lower panel) of the first harmonic as a function of the energy, obtained by ARGO-YBJ, compared with the results of other experiments. (Sakakibara et al. 1973; Gombosi T. et al. 1975; Alexeenko et al. 1981; Cutler et al. 1981; Lagage et al. 1983; Thambyapillai T. 1983; Morello C. et al. 1983; Nagashima et al. 1989; Amenomori et al. 2005b; Munakata et al. 1999; Aglietta et al. 1995, 1996; Swinson et al. 1985; Nagashima et al. 1985; Lee et al. 1987; Andreyev et al. 1987; Ueno et al. 1990; Kuznetsov et al. 1990; Culter et al. 1991; Mori et al. 1995; Fenton et al. 1995; Munakata et al. 1997; Ambrosio et al. 2003; Guillian et al. 2007; Abdo et al. 2008, 2009; Aglietta et al. 2009; Alekseenko et al. 2009; Abbasi et al. 2010, 2012)

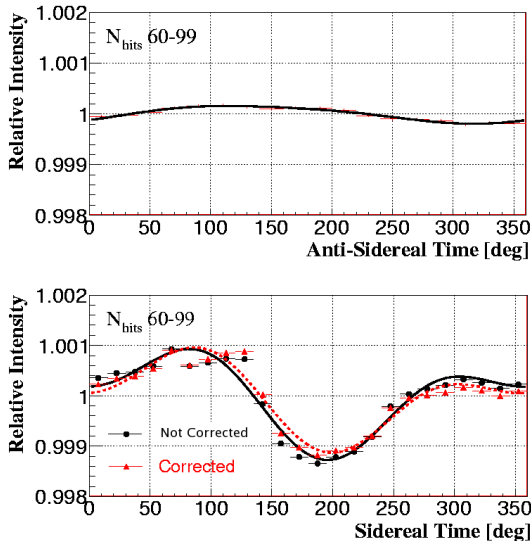


Figure 4. Upper panel: relative intensity of the anti-sidereal distribution for event with $N_{hits}=60-99$. Lower panel: The corresponding sidereal distribution before and after the correction made with the anti-sidereal analysis.

averaging the hour angles of all events with a zenith angle less than 45° , and was found to be 18.6° .

Due to the deep differences between the Equi-Zenith and the East-West method, both in the approach and in handling data, a comparison between them provides a good estimate of systematic uncertainties. In Fig.5, the right ascension projections obtained with the Equi-Zenith and the East-West methods are shown, for events with $N_{hits} > 40$. No significant differences are found between the two distributions and the agreement makes us confident on the reliability of the measurement.

4.2.2. Solar Compton Getting effect

As explained previously, the CG effect was originally proposed as a prediction of a dipolar anisotropy which should be observed in sidereal time because of the motion of the solar system with respect to the CR medium. Such an anisotropy is not the only CG effect that can be investigated. In fact, the Earth itself moves around the Sun and a CG effect should be observed in solar time. Like the sidereal CG effect, the solar CG effect can be predicted with a simple analytical model (Compton & Getting 1935). Given a power law cosmic ray spectrum, the fractional CR intensity variation $\frac{\Delta I}{I}$ is:

$$\frac{\Delta I}{I} = (\gamma + 2) \frac{v}{c} \cos \alpha \quad (4)$$

where γ is the index of the spectrum, v is the Earth's velocity, c the speed of light, and α the angle between the arrival

Table 1

Results of the harmonic analysis for seven N_{hits} intervals. E_m is the median primary energy corresponding to each N_{hits} interval. The column ‘‘Sidereal Time analysis’’ reports the best fit values of the harmonic analysis in sidereal time. The corresponding statistical error are given in the σ_{stat} column. The column ‘‘Anti-sidereal analysis’’ reports the results in anti-sidereal time.

E_m (TeV)	Harmonic vectors	Sidereal Time analysis	$\chi^2/d.o.f$	σ_{stat}	Anti-sidereal analysis
0.98	A_1	6.1×10^{-4}	321/20	0.1×10^{-4}	0.8×10^{-4}
	ϕ_1 ($^\circ$)	42.2		1.0	14.4
	A_2	4.4×10^{-4}		0.1×10^{-4}	0.2×10^{-4}
	ϕ_2 ($^\circ$)	101		0.7	0.5
1.65	A_1	7.9×10^{-4}	280/20	0.1×10^{-4}	0.8×10^{-4}
	ϕ_1 ($^\circ$)	31.7		1.1	11.8
	A_2	5.2×10^{-4}		0.1×10^{-4}	0.2×10^{-4}
	ϕ_2 ($^\circ$)	100		0.8	0.9
2.65	A_1	9.8×10^{-4}	86/20	0.2×10^{-4}	0.8×10^{-4}
	ϕ_1 ($^\circ$)	37.0		1.3	7.8
	A_2	5.4×10^{-4}		0.2×10^{-4}	0.6×10^{-4}
	ϕ_2 ($^\circ$)	100.7		1.2	0.1
4.21	A_1	10.4×10^{-4}	70/20	0.3×10^{-4}	0.2×10^{-4}
	ϕ_1 ($^\circ$)	28.4		1.5	7.1
	A_2	6.1×10^{-4}		0.3×10^{-4}	0.3×10^{-4}
	ϕ_2 ($^\circ$)	103.2		1.3	2.6
7.80	A_1	11.6×10^{-4}	53/20	0.4×10^{-4}	0.4×10^{-4}
	ϕ_1 ($^\circ$)	29.2		1.8	7.2
	A_2	5.2×10^{-4}		0.4×10^{-4}	0.6×10^{-4}
	ϕ_2 ($^\circ$)	102.2		2.0	2.6
13.6	A_1	8.7×10^{-4}	53/20	0.5×10^{-4}	0.5×10^{-4}
	ϕ_1 ($^\circ$)	36.9		3.6	2.7
	A_2	4.4×10^{-4}		0.5×10^{-4}	0.2×10^{-4}
	ϕ_2 ($^\circ$)	94.6		3.6	9.8
29.1	A_1	3.8×10^{-4}	46/20	0.5×10^{-4}	0.4×10^{-4}
	ϕ_1 ($^\circ$)	7.8		7.3	81.2
	A_2	3.9×10^{-4}		0.5×10^{-4}	0.3×10^{-4}
	ϕ_2 ($^\circ$)	88.7		3.6	12.5

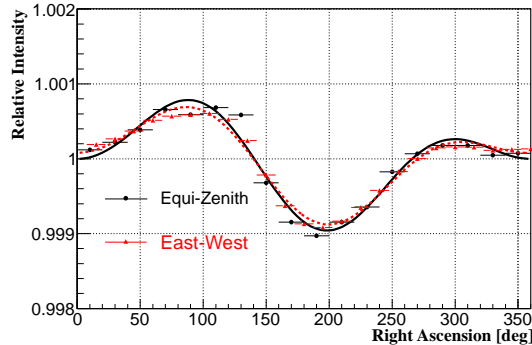


Figure 5. Relative intensity of cosmic rays obtained using the Equi-Zenith method (dots) and the East-West method (triangles), together with the best fit curve obtained with the harmonic analysis.

direction of cosmic rays and the direction of the detector motion, that changes continuously due to the Earth rotation and revolution. Assuming $\gamma = 2.63$ and $v = 30 \text{ km s}^{-1}$, averaging the angle α over one year, the expected signal is a dipole anisotropy with an average amplitude of 3.82×10^{-4} at 6.0 hr of solar time.

Even if the observation of the solar CG effect is less important than the sidereal one (because there is no doubt that CRs do not co-rotate with the Earth around the Sun), nevertheless it gives important indications on the stability of the appara-

tus, and the agreement between observation and expectation would be a strong validator of the detector performance, as well as of the full chain of analysis.

Since the effects of the Sun activity could influence the propagation of cosmic rays up to $\sim 1\text{-}10 \text{ TeV}$, we study the CG signal using events of higher energy. Fig.6 reports the events distribution in solar time compared to the expected one, for showers with $N_{hits} > 500$, which correspond to a median primary energy of 13.7 TeV. The solar CG effect is clearly observed, with an amplitude of $(3.64 \pm 0.36) \times 10^{-4}$ and a phase of $6.67 \pm 0.37 \text{ hr}$ ($\chi^2/d.o.f. = 34.5/16$).

5. SUMMARY AND CONCLUSIONS

This paper reports on the measurement of the large scale anisotropy by the ARGO-YBJ experiment, in the energy range $\sim 1\text{-}30 \text{ TeV}$. The data collected in 2008 and 2009, during a phase of minimum solar activity, have been used to build a two dimensional map of the CR intensity in the declination band $-10^\circ < \delta < +70^\circ$. Two large structures are observed, i.e. an excess region at R.A. = $50^\circ\text{-}140^\circ$ in the direction of the heliotal and a broad deficit at R.A. = $150^\circ\text{-}250^\circ$, in the direction of the Galactic North Pole (R.A. = 192.3° , $\delta = 27.4^\circ$). These observations are in fair agreement with previous results from other experiments also using different techniques, supporting the robustness of the result. In particular, the amplitude of the deficit is consistent with that measured by the Tibet AS- γ array during the previous 8 years.

The high statistics of our sample allowed the detection of

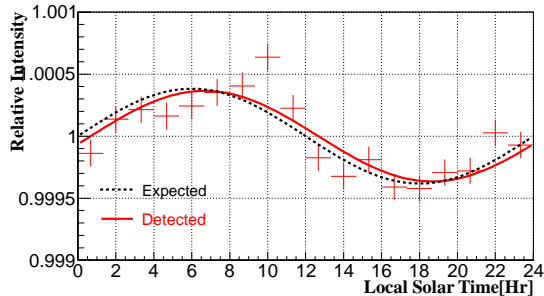


Figure 6. Projection of the event distribution in solar time for $N_{hits} > 500$. The dotted line represents the expected Compton-Getting modulation. The abscissa bars present the wide of bins and ordinate errors are statistical.

many structures of angular size as small as ~ 10 degrees, superimposed to the largest structures. Even neglecting such a small structures, the observed anisotropy is not a pure dipole, and the harmonic analysis of the intensity distribution as a function of the right ascension shows that the data can be described by the first two components of a Fourier series, representing the diurnal and semidiurnal sidereal modulation. The amplitude of the first harmonic is about a factor 1.5 larger than the second one.

The energy dependence of the anisotropy has been studied building two-dimensional sky maps for seven different intervals of events multiplicity with median energies ranging from 1 to 30 TeV. The excess and deficit regions are observed with high significance. The data show that the absolute value of the intensity of both regions increases with energy up to ~ 10 TeV, then decreases, while the position of both the maximum and the minimum slightly shifts towards smaller values of right ascension. The similar energy dependence could suggest that the origin of the excess and deficit regions is the same.

The harmonic analysis shows that the amplitude of the first harmonic increases with energy and doubles in the range ~ 1 to ~ 10 TeV, then decreases. The position of the maximum intensity is consistent with the data of other detectors working in different energy ranges. The general scenario is that first harmonic amplitude increases by a factor ~ 5 in the energy range ~ 100 GeV - 10 TeV, then decreases until the energy reaches ~ 400 TeV, where the phase abruptly changes. The phase observed by ARGO-YBJ is around 3 hr of sidereal time, consistent with the decrease trend observed in the 100 GeV - 300 TeV range. The second harmonic amplitude also shows a similar behaviour, but the variation is smaller.

In conclusion, the ARGO-YBJ data provide accurate observations in the energy range where the anisotropy reaches its maximum intensity, with a set of high statistics data covering more than one decade of energy around this feature. The reliability of the data and the analysis technique has been checked by using the East-West method, that gives consistent results, and with the observation of the solar CG effect at energies above 10 TeV, where the Sun activity effects are expected to be negligible.

The origin of the observed anisotropy is still unknown. Galactic cosmic ray are believed to be accelerated by supernova blast waves and then trapped in the Galactic magnetic fields. Since the strength of the magnetic fields is supposed to be of the order of a few micro-Gauss, the gyro-radii of CRs of energy 1-10 TeV could be of the order of $10^{-2} - 10^{-3}$ pc, much smaller than the thickness of the Galactic disk (~ 200

pc). Hence, the motion of cosmic rays is expected to be randomized and the arrival direction highly isotropical. The observed small anisotropies are likely due to the superimposition of different components that operate at different scales. The distribution of sources, the irregularities of the magnetic field, in particular in the Sun neighbourhood, likely contribute to some extent to shape the cosmic ray spatial distribution. The heliosphere could contribute to model the anisotropy below 10 TeV, with possible effect related to the solar activity. All these components could be disentangled only in the future with more precise measurements exploring in detail the angular structures and the evolution of cosmic rays anisotropies in a wide energy range.

6. ACKNOWLEDGMENTS

This work is supported in China by NSFC (No.11375052, No.10975046, No.10120130794, No.11165013), the Chinese Ministry of Science and Technology, the Chinese Academy of Sciences, the Key Laboratory of Particle Astrophysics, CAS, and in Italy by the Istituto Nazionale di Fisica Nucleare (INFN).

We also acknowledge the essential supports from W.Y. Chen, G. Yang, X.F. Yuan, C.Y. Zhao, R. Assiro, B. Biondo, S. Bricola, F. Budano, A. Corvaglia, B. D' Aquino, R. Esposito, A. Innocente, A. Mangano, E. Pastori, C. Pinto, E. Reali, F. Taurino and A. Zerbini, in the installation, debugging and maintenance of the detector.

REFERENCES

- Aartsen, M. G., Abbasi, R., Abdou, Y., et al., 2013, *ApJ*, 765, 55.
 Abbasi, R., Abdou, Y., Abu-Zayyad, T., et al., 2010, *ApJL*, 718, L194.
 Abbasi, R., Abdou, Y., Abu-Zayyad, T., et al., 2011, *ApJ*, 740, 16.
 Abbasi, R., Abdou, Y., Abu-Zayyad, T., et al., 2012, *ApJ*, 746, 33.
 Abdo, A. A., Allen, B., Aune, T., et al. 2008, *PRL*, 101, 221101.
 Abdo, A. A., Allen, B., Aune, T., et al. 2009, *ApJ*, 698, 2121.
 Aiellia G., Assirob R., Baccic C., et al., 2006, *NIM A*, 562, 92.
 Abeysekara, A.U., Alfaro, R., Alvarez, C., et al. 2014, *ApJ*, 796, 108.
 Aglietta M., Alessandro B., Antonioli P. et al., 1995, *Proc. of the 24th ICRC*, Rome, IT; 2, 800.
 Aglietta M., Alessandro B., Antonioli P. et al., 1996, *ApJ* 470, 501.
 Aglietta, M.V., Alekseenko, V., Alessandro, B., et al., 2009, *ApJ*, 692, L130.
 Alexeenko, V. V., Chudakov, E. A., Gulieva, N. E., & Sborshikov, G. V. 1981, in *Proc. 17th ICRC*, Paris, 2, 146.
 Alekseenko V.V., Cherniaev A.B., Djappuev D.D., et. al., 2009, *Nuclear Physics B*, 196, 179-182.
 Ambrosio M., Antolini R., Baldini A. et al., 2003, *Phys. Rev. D*, 67, 042002.
 Amenomori, M., Ayabe, S., Cui, S. W., et al. 2005, *ApJ*, 633, 1005.
 Amenomori, M., Ayabe, S., Cui, S. W., et al. 2005, *ApJ*, 626, L32.
 Amenomori, M., Ayabe, S., Bi, X. J., et al. 2006, *Science*, 314, 439.
 Amenomori, M., Bi, X. J., Chen, D., et al. 2010, *ApJ*, 711, 119.
 Amenomori, M., Bi, X. J., Chen, D., et al. 2012, *Astrop. Phys.*, 36, 237.
 Andreyev Y.M., Chudakov A.E., Kozyarivsky V. A. et al., 1987, *Proc. 20th ICRC*, Moscow, URSS; 2, 22.
 Antoni, T., Apel, W. D., Badea, A. F., et al., 2004, *ApJ*, 604, 687.
 Bartoli, B., Bernardini, P., Bi, X. J., et al., 2011, *Phys. Rev. D*, 84, 022003.
 Bartoli, B., Bernardini, P., Bi, X. J., et al., et al., 2013, *Phys. Rev. D*, 88, 082001.
 Bartoli, B., Bernardini, P., Bi, X. J., et al., 2014a, *Phys. Rev. D*, 89, 052005.
 Bartoli, B., Bernardini, P., Bi, X. J., et al., 2014b, *ApJ*, 790, 192.
 Bartoli, B., Bernardini, P., Bi, X. J., et al., 2014c, *ApJ*, 779, 27.
 Bartoli, B., Bernardini, P., Bi, X. J., et al., 2014d, *Chinese Phys. C*, 38, 045001.
 Bartoli, B., Bernardini, P., Bi, X. J., et al., 2015, *ApJ*, 798, 119.
 Bonino, R., Alexeenko, V.V., Deligny, O., Ghia, P.L., 2011, *ApJ*, 738, 67.
 Compton, A. H., Getting, I. A., 1935, *Phy. Rev. Lett.*, 47, 817.
 Cutler, D. J., Bergeson, H. E., Davies, J. F., & Groom, D. E., 1981, *ApJ* 248, 1166.
 Cutler, D. J., & Groom, D. E., 1991, *ApJ*, 376, 322.
 Drury, L., Aharonian, F., 2008, *Astroparticle Physics* 29, 420.

- Di Sciascio G. and Iuppa R., "On the observation of the Cosmic Ray Anisotropy below 10^{15} eV", in "Homage to the Discovery of Cosmic Rays, the Meson-Muons and Solar Cosmic Rays", Chapter 9, pagg. 221-257 (Nova Science Publishers, Inc., New York, 2013), Preprint: arXiv:1407.2144.
- Fenton, K. B., Fenton, A. G., Humble, J. E. 1995, Proc. 24th ICRC, Roma, IT; 4, 635.
- Gombosi, T., Kota, J., Somogyi, A. J. et al., 1975, Proc. of the 14th ICRC, West Gemany, vol. 2, p. 586.
- Guillian, G., Hosaka, J., Ishihara, K., et al. , 2007, Phys. Rev. D, 75, 062003.
- Guo, Y.Q., Zhang, X.Y., Zhang, J.L., et al., 2010, Chinese Physics C, 34(5), 555.
- Heck D. et al. CORSIKA: A Monte Carlo Code to Simulate Extensive Air Showers, Forshungszentrum Karlsruhe, FZKA 6019 (1998) and references therein.
- Kuznetsov A. V., 1990, Proc. 21st ICRC, delaide 6, 372.
- Lagage P.O. and Cesarsky C.J., 1983, A& A., 125, 249.
- Lee Y.W. and Ng L.K., 1987, Proc. 20th ICRC, Moscow, URSS; 2, 18.
- Li, T. L., Liu, M. Y., Cui, S. W., Hou, Z. T., 2012, Astroparticle Physics, 39-40, 144.
- Morello C. et al., Proc. of the 18th ICRC, Bangalore, IN; 2, 137.
- Mori S., Yasue S., Munakata K. et. al, 1995, Proc. 24th ICRC, Rome, IT; 4, 648.
- Munakata, K., Mizoguchi, Y., Kato, C., et al., 2010, ApJ, 712, 1100.
- Munakata K., Kiuchi T., Yasue S., et al., 1997, Phys. Rev. D, 56, 23.
- Munakata K., Hara T., Yasue S. et al., 1999, Advances in Space Research, 23, 611-615.
- Nagashima, K., Fujimoto, K., & Jacklyn, R. M., 1998, J. Geophys. Res., 103, 17429.
- Nagashima, K., Sakakibara, S., Fenton, A. G., & Humble, J. E. 1985, Planet. Space Sci., 33, 395.
- Nagashima K., FUJIMOTO K., SAKAKIBARA S., et al., 1989, Nuovo Cimento C, 12, 695.
- Nolan, P. L., Abdo, A. A., Ackermann, M., et al. 2012, ApJS, 199, 31
- Qu X.B., Zhang Y. , Xue L., Liu C. et al., 2012, ApJL, 750,1.
- Salvati, M., Sacco, B., 2010, A&A 513, A28.
- Sakakibara S. et al., 1973, Proc. 13th ICRC, Denver, USA; 2, 1058.
- Schwadron, N. A., Adams, F. C., Christian, E. R., et al. 2014, Science, 343:988.
- Swinson D.B. and Nagashima K., 1985, Planet Space Sci., 33, 1069.
- Thambyaphillai T., 1983, Proc. 18th ICRC, Bangalore, IN; 3, 383.
- Ueno, H., Fujii, Z., & Yamada, T. 1990, Proc. 21st ICRC, delaide, 6, 361.
- Zhang, J.L., on behalf of ARGO-YBJ collaboration, 2009, in Proc. 31st ICRC, Lodz-Poland.
- Zhang, M., Zuo, P.B., and Pogorelov, N., 2014, ApJ, 790, 5.